RSC Advances

ROYAL SOCIETY OF CHEMISTRY

www.rsc.org/advances

Dense Inter-particle Interaction Mediated Spontaneous Exchange Bias in NiO Nanoparticles

Ashish Chhaganal Gandhi[a,b], Jayashree Pant[c] , and Sheng Yun Wu[*,a]

[a]Department of Physics, National Dong Hwa University, Hualien 97401, Taiwan

[b]Center for Condensed Matter Sciences, National Taiwan University, Taipei, Taiwan

[c]Department of Physics, Abasaheb Garware College, Savitribai Phule Pune University, India

Abstract

We report the finite size effect and nickel vacancy defects in NiO nanoparticles that result in the formation of magnetic phase separation in uncompensated antiferromagnetic NiO-cores with frustrated and disordered spins at the surface NiO-shell. The inter-particle interaction is probed by analyzing the relaxation dynamics measurements. A significant index for the interaction of *n* derived from the dynamic magnetization is proposed, which paves the way for the examination of the spontaneous exchange bias mechanism and offers insight into the influence of the particle size and defects.

Keywords: nanoparticles; antimagnetic; ferromagnetic; spontaneous exchange bias

*Corresponding author:sywu@mail.ndhu.edu.tw (SYW)

1. INTRODUCTION

Nickel oxide (NiO) is an antiferromagnetic (AFM) insulating material having a Néel temperature (T_N = 520 K) above room temperature which has been the object of extensive research attention over the last few decades because of its importance in numerous technological applications (i.e., catalysis, batteries, ceramics etc.). In the last decade, renewed interest has been generated in nanoscale NiO whose unique properties (i.e., high surface to volume ratio, short diffusion paths, enhanced magnetic and electric properties, nickel vacancies etc.) have opened up avenues for its use in diverse fields for catalysis[1-3], anodic electrochromics[4], capacitors[5,6], smart windows[7], fuel and solar cells[8,9], biosensors[10] and spintronics[11-13]. In particular, intense research effort is being made to combine NiO nanostructures with graphene in order to develop highly functional energy storage systems[14,15] and electrochemical sensors[16]. Saha *et al.*[17] first explained the zero-field or spontaneous exchange bias (EB) effect by using a micromagnetic simulation in a bilayer system with a polycrystalline AFM. The term *spontaneous* refers to the case in which the system is not conventionally field cooled. They proposed a mechanism which could induce unidirectional anisotropy (UA) in an otherwise isotropic ferromagnetic–antiferromagnetic (FM-AFM) system just by the simple application of the first field point in the hysteresis loop evaluation without setting any initial bias as was used to observe the spontaneous exchange bias (SEB) effect. Recently, the SEB effect has been observed in various bulk, FM/AFM core/shell, and nanocomposite to pure AFM nanostructure systems. For example, Maity *et al.*[18] reported on superspinglass mediated giant SEB (300-600 Oe) in an AFM-FM $BiFeO_3$-$Bi_2Fe_4O_9$ nanocomposite. They ascribed the observed SEB to spontaneous symmetry breaking and the consequent onset of UA driven by "super interaction bias coupling" between the FM core of $Bi_2Fe_4O_9$ (~19 nm) and the canted AFM moment in the coarser

$BiFeO_3$ (~112 nm) through superspin-glass moments at the interface. Similarly, Lierop *et al.*[19] observed SEB in $Ni_{80}Fe_{20}/Co_3O_4$ thin films. Liu *et al.*[20] also observed an absence of AFM state in α-Fe_2O_3 nanocrystals. In their comprehensive measurements and analysis, all the as-synthesized products for different morphologies illustrate magnetic phase transformation at extremely low temperatures, and show no apparent Morin transition in the range 2 to 350 K. We note that, in all the above examples the observed SEB is due to UA driven by coupling at the interface of the FM-AFM component. Ahmadvand *et al.*[21] observed SEB in AFM $LaFeO_3$ nanoparticles (40 to 45 nm) attributing it to exchange coupling between the weak-FM shell and the AFM core of the particles. Chauhan *et al.*[22] reported on the effect of varying particle sizes and maximum applied fields during the initial magnetization on the SEB in AFM hexagonal-$YMnO_3$ nanoparticles (45 to 90 nm). The observed SEB was attributed to the exchange interaction between the compensated AFM spins and spin-glass-like uncompensated surface spins. In this work, we present that in AFM NiO nanoparticles the inter-coupling between short-range ordered clusters of spins which behave like weak ferromagnetic (FM) NiO-shells and uncompensated AFM NiO-cores lead to a shift in the hysteresis loop known as the SEB phenomenon. To study the anomalous magnetic behavior of AFM NiO nanoparticles, static and dynamic magnetic measurements, including time, temperature and field dependence have been carried out.

2. EXPERIMENTAL DETAILS

The structural and morphological analysis of chemically synthesized 16.6(7), 19.5(6), 29(4), 31(1), and 54(6) nm NiO particles has been discussed in detail in our previous work[23]. Nanoparticles of NiO were synthesized by the sol-gel technique followed by annealing in an ambient atmosphere for 1 hour at different temperatures from 400 to 800 ℃ (at intervals of

100 ℃). In a previous work, we utilized confocal Raman spectroscopy to probe the superexchange interaction energy E_{2M} along the next-nearest-neighbor (NNN) Ni^{2+} ions through oxygen in NiO. The observed exponential decrease of E_{2M} with particle size was attributed to an increase in the nickel vacancy concentration. In this work we probe the effect of the nickel vacancy concentration and finite size on the magnetic properties of NiO nanoparticles. Detailed temperature, time and field dependent magnetic measurements were carried out using a superconducting quantum interference device (SQUID) magnetometer (Quantum Design, VSM). The morphology was characterized using a transmission electron microscope (TEM, JEM-3010 JEOL) and structural characterization was made from high-resolution TEM (HRTEM) and selective area diffraction patterns (SAED) of all the NiO nanoparticles.

3. RESULTS AND DISCUSSION

3.1. Morphology and structural analysis

The TEM images in **Figures 1(a)-(e)** show the morphology for NiO nanoparticles with various annealing temperatures ranging from 400 to 800 ºC, respectively. It can be seen that the nanoparticles obtained after annealing at T_A = 400 °C, as shown in **Figure 1(a)**, are closely packed and irregular in shape. The effect of further thermal treatments at 500 to 800 °C, resulted in an increase in both the size and dispersity of the nanoparticles. Details about the mean diameter estimated by using a log-normal distribution function and the grain size obtained from a Williamsons-Hall plot have been discussed in our previous work[23]. Annealing at low temperature (400 to 600 °C) resulted in the formation of particles with a single domain having grain sizes of 16.6(7), 19.5(6) and 29(4) nm, respectively. Further

annealing at higher temperatures, 700-800 °C resulted in the formation of particles with multiple grains having grain sizes of 31(1) and 54(6) nm, respectively. The NiO nanoparticles of all the samples seemed to be pseudo-spherical in shape and retained a perfect $Fm\bar{3}m$ crystalline structure as can be seen in the HRTEM images shown in the inset to **Figures 1(a)-(e)**). The inter-planar distance *d* obtained from HRTEM images of 400-800 °C annealed particles are 2.101, 2.095, 2.091, 2.087, and 2.085 Å, respectively, corresponding to the [200] nuclear plane of NiO nanoparticles. The lattice constants (4.202, 4.189, 4.182, 4.174, and 4.170 Å) calculated from the *d* value for the particles annealed at 400-800 °C matched the XRD analysis very well[22]. The observed increase in the lattice constants with the decrease of particle size can be attributed to the effect of nickel vacancy defects and finite size effects, details about which have been discussed in our previous report[23]. The selective-area-electron-diffraction (SAED) patterns of particles annealed at 400-600 ℃ reveal their poly-crystalline nature; see **Figures 1(f)-(h)**. The SAED patterns of large sized 31(1) and 54 (6) nm NiO particles appearing in **Figures 1(i)-(j)** can be ascribed to the existence of cubic NiO along the [001] and [111] reflection zone axes.

3.2. Temperature Dependent Magnetic Measurement

The temperature dependence of the field cooling (FC) and zero field cooling (ZFC) magnetization for NiO nanoparticles with a mean diameter 16.6(7) nm with a applied magnetic field H_a=100 Oe is shown in **Figures 2(a)**. The ZFC magnetization shows a pronounced board peak, defined as a blocking temperature T_B ~178 K, while FC magnetization increases monotonically with decreasing temperature below T_B. At lower temperature, there is a small peak in the ZFC magnetization visible at around 6 K, called as the freezing temperature T_f which is associated with collective freezing of uncompensated

surface NiO moments. A value of T_f ranging from 5 to 15 K has been reported for NiO nanoparticles synthesized by different techniques[24-31]. As shown in **Figure 2(a)**, a bifurcation between the ZFC and FC is visible above T_B with the data beginning to merge at an irreversible temperature T_{irr}. The sizes dependence of T_B , T_{irr} and T_f are depicted in **Figure 2(b)**, respectively, whereas T_f reveals size independent. The values of T_B and T_{irr} show a further increase of particle size from 16.6(7) to 31(1) nm for a shift in the T_B from 198 K to 374 K, and the T_{irr} from 262 to 398 K, respectively. The similar increasing behavior of T_B with the size has also been observed from small size NiO nanoparticles (< 10 nm). Duan *et al.*[31] reported an increase of T_B from 19.8 to 161 K with increase in the particle size from 3.5 to 12.4 nm. Similarly, Montes *et al.*[32] reported an increase of T_B ~ 3.5, 53 and 145 K with particle size, 2 to 10 nm. However, Thota *et al.*[26] reported an increase of T_B and T_{irr} with a decrease of particle size from 22 to 4.1 nm. In the former two studies, it was observed that the set of nanoparticles are non-interacting, whereas in later findings they are interacting. Shim *et al.*[25] compared the size dependency of T_B from non-interacting (oleic acid (OA) coated) and interacting (uncoated) NiO particles (5 to 20 nm). An increase in T_B with size was observed from all the OA coated, non-interacting nanoparticles. In contrast, a decrease of T_B with an increase of particle size up to 8 nm and above, and an increase with size was observed from uncoated nanoparticles. Their findings confirmed that the value of T_B from NiO nanoparticles is not just governed by the size and distribution of the particles, but also by their nature. The observed increase of T_B with particle size signals that the inter-particle interaction in this set of nanoparticles is either weak or absent, which will be discussed later in the text.

In addition, the magnetic susceptibility of the bulk AFM material increases with temperatures below the Néel temperature but exhibits paramagnetic behavior[33]. The observed decrease in magnetization (from both ZFC-FC curves) with measurement temperature for

31(1) nm particles (see supporting information: **Figure S1(a)**) indicates that the AFM moments begin to dominate over the net magnetization. The 54(6) nm (T_A = 800 ℃) particles show bulk-like AMF behavior (see supporting information: **Figure S1(b)**). A similar increase of magnetization with temperature has been reported by Richardson *et al.*[34] from bulk NiO and by Mandal *et al.*[33] from quenched NiO particles (size ≥ 60 nm). However, recently Mariana *et al.*[35] observed paramagnetic behavior over temperatures ranging from 2–380 K from 60.3 ± 2.2 nm NiO particles. The observed behavior was attributed to incomplete compensation of the AFM sublattices at the surface. They claimed that the paramagnetic behavior observed from the nanoparticles is typically the same as that observed from bulk NiO, citing references to Jagodič *et al.*[36] and Winkler *et. al*[25]. However, Jagodič *et al.*[36] observed a similar kind of surface spin magnetization effect from both nanoparticles and bulk NiO, but only below 25 K. A further increase of measurement temperature of bulk NiO resulted in an increase of susceptibility similar to that observed in **Figure S1(b)** (see supporting information). On the other hand, Winkler *et al.*[25] reported observation of the paramagnetic behavior in the high temperature region in 3 nm sized NiO particles which was attributed to highly uncompensated moments of the AFM core. The 3 nm size particle is ~ 20 times smaller and at such a small size nickel vacancy defects are too high, resulting in paramagnetic/superparamagnetic behavior due to the breakdown of AFM ordering[32]. This argument is consistent with the recently observed breakdown of AFM ordering in ~ 2.5 nm NiO particles by Montes *et al*[32]. We also observed a similar breakdown of AFM ordering in the ~ 3 nm size NiO nanoparticles (data not published). Furthermore, the $M(T)$ behavior for 3 nm size particles is similar to that observed by Jagodič *et al*[36] and Duan[31] and Montes [32], due to freezing of the clusters of surface spins. The $M(T)$ behavior observed from the R-sate of samples (size ≥ 60 nm) by Proenca *et al.*[35] is similar to that observed by Mandal *et al.*[33] and they speculate on the existence of two components, FM and/or paramagnetic and AFM. The

former dominates in the low temperature region and the latter in the high temperature region. Furthermore, the invisibility of T_f for the <d>=54(6) nm sample strongly suggests the absence of disordered surface moments and nickel vacancies. Therefore, NiO particles with a crystalline size higher than or equal to 54(6) nm behave like bulk NiO and can be considered as ideal AFM NiO[32]. Furthermore, the value of the magnetization (M_{FC}) decreases with the increase of particle size. The observed increase of susceptibility to a decrease of NiO nanoparticle size is in good agreement with the results of Tiwari *et al*.[27]

The finite size effect results in disordered spins at the surface were concluded in our previous work from the analysis of two magnon excitation[23, 37]. The intensity of magnon excitation in NiO is related to AFM ordering and it decreases with the increase of nickel vacancy concentration[38]. There is a monotonic increase in the nickel vacancies with a decrease in the particle size. Therefore, each uncompensated AFM NiO nanoparticle gives rise to a net magnetic moment due to a reduction in the number of exchange coupled moments caused by finite size effects. In such a scenario, at finite temperatures, the uncompensated AFM exhibits superparamagnetic (SPM) behavior. The important characteristic of SPM is the superparamagnetic relaxation time, also called the Néel relaxation time τ_N[39]. The τ_N is the average time that the magnetization spends in the minima of the anisotropic energy. Let us consider an assembly of particles with uniaxial anisotropy along the *z*-axis. A large external field H_a is applied along the *z* direction, such that all the particles are magnetized to saturation M_S. If the field is removed, the magnetization will decay due to thermal agitation according to the relationship $M_S = M_o \exp(-t/\tau)$. If τ_N is very large, $M_S = M_o$ and the system will remain in a stable state. The relaxation time τ_N then must be proportional to the Boltzmann's factor, $\exp(E(\theta)/k_BT)$, since $E(\theta) = KV\sin^2(\theta)$ is the energy barrier between the two energy minima. Thus, the relaxation rate can be written as

follows: $\tau_N = \tau_o \exp(KV/k_BT)$, where K is the magnetic anisotropic energy density, V is the particle volume, k_B is Boltzmann's constant, and τ_o is the characteristic of the material, called the attempt time, with a typical value in the range of 10^{-13} to 10^{-9} s. At a certain temperature, T_b, τ_N will become equal to τ_m, the time of measurement. This leads to $T_b = (KV/k_B)/\ln(\tau_m/\tau_o)$ and it then becomes dependent on the measurement time. According to the Néel-Brown model[39, 40], the uniaxial and non-interacting SPM nanoparticles exhibit distribution in the anisotropic energy barrier due to poly-dispersity. In this work, the experimental measurement time is τ_m = 4 s, and $\tau_o \sim 10^{-9}$ s, then $T_B \approx KV/22k_B$. Using the above expression, the calculated K shows exponential dependency on the nanoparticle volume as shown in **Figure 3** (summarized in **Table 1**). Furthermore, the solid black line in **Figure 3** indicates the Néel-Brown model, which fits T_B versus V plotted for large size particles using K = 72864 erg/cm^3 (K value of 31(1) nm nanoparticles) very well. However, the data points of small size particles (16.6(7) nm and 19.5(6) nm) show significant deviation from linearity and extrapolation to the vertical axis shows a non-zero value even at zero volume. The non-zero value could be due to the inter-particle interaction as small size particles are poly-dispersed, densely packed (as seen from SEM/TEM) and possess the highest amount of nickel vacancies.

3.3. Relaxation dynamics

Ulrich *et al.*[41] proposed a theoretical model for the characterization of nanoparticle systems involving inter-particle interaction or a spin-glass like behavior. The decay of magnetization relaxation of intermediate and large concentrated poly-dispersed FM particles over time explicitly follows the power law $W(t) = t^{-n}$, where $W(t) = -(d/dt)\ln M(t)$. The value of n

defines the state of the system, i.e., if n = 0, then it is a dilute system of mono-dispersed particles, $n \sim 2/3$ is a dilute system of poly-dispersed particles, and $n \geq 1$ becomes a dense system, independent of size distribution. This theoretical model is based on Monte Carlo simulations and has been used frequently for interpretation of the relaxation dynamics of magnetic clusters[42-43] and nanoparticles[45-47]. The model is useful to probe the strength of the interparticle interactions. To examine the interparticle interaction time dependent magnetization relaxation M(t) measurement was carried out within the blocking state. First, the sample was cooled down from 300 K to 60 K in a small external magnetic field of 100 Oe. Subsequently, the magnetic field was turned off using an oscillator mode (rate 10 Oe/s) and relaxation of the magnetic moment with respect to time was recorded for a time period of one hour. **Figure 4** shows the plot of $\ln W(t)$ verses $\ln(t)$ for various sizes of NiO nanoparticles. The solid line represents the fit obtained using $\ln W(t) = c - n\ln(t)$ and the fitting parameters are depicted. The fitted value of n = 0.93 for the smallest size particles, 16.6(7) nm lies within the dilute system of poly-dispersed particles and dense system of strongly interacting particles. The poly-dispersity is due to the broad size distribution of particles as observed from log-normal fitting and it narrows down with an increase of particle size. As seen from the ZFC-FC measurements, these particles possess the highest magnetic moment and therefore exhibit strong interaction. The value of the relaxation rate n decreases with an increase of particle size, and for 54(6) nm NiO particles it becomes time independent, which is characteristic of an ideal AFM material. For particles with sizes higher than ~ 30 nm we obtain qualitatively the same picture as for mono-dispersed systems. Therefore, we can conclude that small size particles are densely packed, poly-dispersed and possess the highest magnetic moment. The enhanced magnetic moment in small size particles could arise from spontaneously formed short-range ordered clusters of spins at the surface in an applied

magnetic field, which lose their magnetization with the passage of time and therefore can be regarded as a weak-FM material.

3.4 Spontaneous Exchange Bias Phenomenon

Spontaneous exchange bias (SEB) results from a break in the symmetry across the FM-AFM interface and setting up of the UA during the first field of hysteresis loop measurement. To study the SEB phenomenon magnetization versus applied magnetic field, M(H_a) was measured using a *p*-type protocol, 0 → (+H_{max})→ (-H_{max})→ (+H_{max}) in ZFC mode at 25 K, as shown in **Figure 5**. The M(H_a) loop from 16.6(7) nm particles is highly asymmetric, and shifted toward the negative magnetic axis as can be seen from the portion of the loop near the origin in **Figure 5(a)**. The non-zero value of the coercivity (H_C) and remanence (M_r) in the low field region clearly point to the existence of a weak-FM component. Care has been taken to avoid a spurious shift from the trapped magnetic field in a superconducting magnet by demagnetization using a low oscillatory field. The loop asymmetry along the applied field axis and magnetization axis can be quantified as a spontaneous exchange bias field $\left(H_{SEB} = \left(\left|H_{C1}\right| - \left|H_{C2}\right|\right)/2\right)$ and vertical shift $\left(M_{VS} = \left(\left|M_{r1}\right| - \left|M_{r2}\right|\right)/2\right)$, respectively, where H_{C1} and H_{C2} are the fields corresponding to the points in the forward and reverse branches of the hysteresis loop at where the magnetization reaches zero. Similarly, M_{r1} and M_{r2} indicate the magnetization corresponding to the points on the forward and reverse branches of the hysteresis loop at which the applied field is zero. The observed shifts in H_{SEB} and M_{VS} for 16.6(7) nm particles at 25 K are -48 Oe and 1.394×10^{-3} emu/g, respectively. Observation of the SEB field in the AFM transition metal oxides has not yet been reported on, and this is the first report on NiO nanoparticles.

In order to explore the effect of field direction on SEB, we also performed M(H_a) measurements at 25 K with the *n*-type protocol, 0 → (-H_{max})→ (+H_{max})→ (-H_{max}). Similar to the *p*-type, the M(H_a) loop of the *n*-type is also found to be highly asymmetric, but shifted toward the positive magnetic axis, as can be seen in the portion of the loop near the origin in **Figure 5(a).** The observed shifts in H_{SEB} and M_{VS} are 45 Oe and - 1.247×10^{-3} emu/g, respectively. Slightly lower values of H_{SEB} and M_{VS} are obtained after the *n*-type measurements than those of the *p*-type. Maity *et al.*[18,48] reported H_{SEB} of - 850 Oe and + 615 Oe after *p*- and *n*-type hysteresis loop measurements from the $Bi_2Fe_4O_9$-$BiFeO_3$ FM/AFM system, respectively. The slight difference observed in the behavior of SEB field obtained using the *p*-and *n*-type protocols is a common phenomenon. The reported high value of SEB from $Bi_2Fe_4O_9$-$BiFeO_3$ as compared to NiO is due to the inter-coupling between the log-range ordered FM and AFM spins at the interface[18,48]. Furthermore, the *p*-type and *n*-type M(H_a) loops measured in the ZFC mode are almost symmetric in nature and exhibit a similar value for SEB, which is within the experimental measurement error. The above findings indicate that the observed spontaneous shifts in the M(H_a) loop are not experimental artifacts, but rather an intrinsic property of NiO nanoparticles induced by the finite size effect. The corresponding full hysteresis loop measured at 25 K with *p*-type and *n*-type protocols with ZFC is shown in **Figure S2** (see supporting information). From the M(H_a) loops, it can be inferred that in the high field region, magnetization increases linearly with a magnetic field without saturation. The sample consisted of two magnetic components: the first component is easily magnetized in the low-field region and the second non-saturating component is responsible for the linear increasing behavior of magnetization in the high field region. A similar two-component behavior has been reported from different sized NiO nanoparticles[33]. Similarly, the M(H_a) loop measurement for various sizes of NiO nanoparticles was carried out at 25 K by both the *p*- and *n*-type protocols. **Figures 5(b)-(e)** show a portion of the M(H_a)

loop near the origin and **Figures S2(b)-(e)** (see supporting information) show the full hysteresis loop measured with *p*- and *n*-type protocols after ZFC measurement of 19.5(6) nm to 54(6) nm NiO nanoparticles. Non-zero coercivity, loop shift and two component behaviors are visible to the naked eye even for the 19.5(6) nm nanoparticles with reduced values and magnetization compared to that of 16.6(7) nm NiO nanoparticles. As expected, with an increase of particle size, the AFM component overcomes the FM component due to reduced number of nickel vacancies and the surface effect, and the M(H_a) curve exhibits a linear increase of magnetization with the field. The M(H_a) loops for nanoparticles ≥ 30 nm exhibit zero-coercivity and a linear increase in the magnetization, the same as for the bulk AFM material. We note that the value of the magnetization decreases monotonically with the increase in the particle size, which is in excellent agreement with the decrease of nickel vacancies observed in the Raman measurements[23]. The particle size dependency of H_{SEB} observed at 25 K is shown in **Figure 5(f)**. Considering that 10 Oe is the error limit of the magnetic field for the MPMS-SQUID magnetometer, the H_{SEB} decreases with an increase of particle size. As expected, the 31(1) and 54(6) nm NiO nanoparticles do not show any SEB, due to the reduction of the FM component.

To further study the effect of temperature on SEB and the corresponding H_C, the ZFC M(H_a) loop measurement was carried out on a 16.6(7) nm sample at different temperatures, namely, 2, 25, 50, 100, 200 and 300 K, using both the *p*- and *n*-type protocols; see **Figure S3(a)** and **Figure S4(a)** (see supporting information), respectively. The M(H_a) loops measured with both protocols are quite similar showing that the two component behavior exists even up to room temperature. We note that the magnetization at ± 15 kOe increases with temperature, showing a maximum for M(H_a) at 100 K and then decreases, reaching a minimum for M(H_a) at 300 K. In general, for FM materials, the magnetization should

decrease, whereas for AFM materials, it should increase with an increase of thermal energy. The reasons for the observed anomalous behavior are not clear yet and further study needs to be done. The measured M(H_a) loop for the remaining samples, the 19.5(6), 29(4), 31(1) and 54(6) nm nanoparticles with the *p*- and *n*-type protocols at 2, 25, 50, 100, 200 and 300 K are shown in **Figures S3(b)-(e)** and **Figures S4(b)-(e)** (see supporting information), respectively. The M(H_a) loop measured with both *p*- and *n*-type protocols for nanoparticles ≥ 30 nm in size shows a linearly increasing behavior, the same as for the bulk AFM material. Furthermore, the magnetization at ± 15 kOe increases with temperature, showing a maximum for M(H_a) at 300 K, which is consistent with the increasing susceptibility behavior of the pure AFM material. Similar to H_{SEB} and M_{VS}, the values of the coercivity H_C and remanence M_r were obtained from the *p*- and *n*-type M(H_a) loops by using $\left(H_C = \left(\left|H_{C1}\right| + \left|H_{C2}\right|\right)/2\right)$ and $\left(M_r = \left(\left|M_{r1}\right| + \left|M_{r2}\right|\right)/2\right)$, respectively. The temperature dependencies of H_{SEB}, H_C, M_{VS}, and M_r for all the NiO samples are shown in **Figures 6(a)-(d)**. The shaded area represents the maximum instrumental error. In the conventional exchange bias for mono-dispersed FM/AFM core/shell nanoparticles, the values of H_{SEB} decrease with the increase of temperature and vanish above the blocking temperature[49]. In contrast, the reason for the non-zero values observed at 300 K, particularly from small size particles above T_B is not yet clear but could possibly be due to the broad size distribution of the nanoparticles. Furthermore, the H_{SEB} and M_{VS} as a function of temperature show a deep valley around 50 K in the *p*-type M(H_a) loop, and a broad maximum around 25 and 100 K in the *n*-type M(H_a) loop for the 16.6(7) and 19.5(6) nm nanoparticles, respectively. The edge of the shift in the hysteresis loop occurs with NiO nanoparticles with a size of 29(4) nm; the SEB loop shift disappears with particles above this size, which could be due to reduced FM component.

As can be noted in **Figures 6(b)-(d)**, the temperature dependency of H_C and M_r (from both *p*- and *n*-type M(H_a)) shifts to higher temperatures with the increase of particle size. For 16.6(7) nm, H_C and M_r show an increasing behavior with a tendency to bend in the low temperature region. A broad maximum is observed around 100 and 200 K in the M(H_a) loop for the 19.5(6) and 29(4) nm nanoparticles, respectively. Maity *et al*.[48] also observed a similar deep valley for SEB and coercivity around ~150 and 50 K, respectively, from the $Bi_2Fe_4O_9$-$BiFeO_3$ FM-AFM nano-composites. Even though the reason for this deep valley (broad maximum) after the *p*-type (*n*-type) is not clear, the observed loop shift and tendency to approach to zero with temperature confirms the existence of the SEB phenomenon in small size NiO nanoparticles. To further confirm the SEB phenomenon, we also carried out field cooled (FC) hysteresis loop measurement from 0 to 20 kOe. The measurements were performed on 16.6(7) nm NiO nanoparticles which were cooled down from 300 K to 60 K in an external magnetic field. The observed M(H_a) loop (see supporting information: **Figure S5**) shows an asymmetric diagonal loop shift. The observed results clearly show that the external cooling field pre-magnetizes the sample and therefore produces a giant CEB field.

4. CONCLUSIONS

In summary, the size dependency of the blocking temperature and freezing temperature confirm the occurrence of a two-component behavior from the uncompensated AFM NiO and randomly oriented surface spins, respectively. The relaxation dynamic results reveal that 16.6(7) and 19.6(5) nm are dense/poly-dispersed interacting nanoparticles, 29(4) nm: dilute, poly-dispersed, non-interacting nanoparticles and 31(1) and 54(6) nm are dilute, mono-dispersed, non-interacting nanoparticles. The zero-field-cooled hysteresis loop measured using both the *p*-type and *n*-type protocols confirm the initial field direction

dependency of the hysteresis loop shift. The maximum H_{SEB} = -53 Oe and M_{VS} = 1.943 × 10^{-3} emu/g at 50 K and H_C = 903 Oe and M_r = 0.03251 emu/g at 2 K were obtained for the *p*-type M(H_a) loop of a 16.6(7) nm NiO nanoparticles. The values of H_{SEB}, M_{VS}, H_C and M_r decrease with the increase of particle size due to reduction of the FM component (i.e., decrease of nickel vacancy concentration). The observed SEB effect is attributed to the inter-coupling of spins at the interface of short-range ordered clusters of spins, which behave like weak FM to the uncompensated AFM.

AUTHOR'S INFORMATION

***Corresponding Author's E-mail:** sywu@mail.ndhu.edu.tw

ACKNOWLEDGMENTS

We would like to thank the Ministry of Science and Technology (MOST) of the Republic of China for their financial support of this research through project numbers MOST-103-2112-M-259-005 and MOST-104-2112-M-259-001.

REFERENCES

[1] J. Park, E. Kang, S. U. Son, H. M. Park, M. K. Lee, J. Kim, K. W. Kim, H. J. Noh, J. H. Park, C. J. Bae, J. G. Park and T. Hyeon, *Adv. Mater.* 2005, **17** 429-434

[2] J. Xiao, B. Chen, X. Liang, R. Zhang and Y. Li, *Catal. Sci. Technol.*2001, **1** 999-1005

[3] Y. –H. Pai and S. –Y. Fang, *J. Power Sources* 2013, **230** 321-326.

[4] E. L. Runnerstrom, A. Llordes, S. D. Lounis and D. J. Milliron, *Chem. Commun.2014,* **50** 10555-10572.

[5] X. Yan, X. Tong, J. Wang , C. Gong, M. Zhang and L. Liang, *Mater. Lett.* 2013, **95** 4.

[6] Jahromi S. Pilban, A. Pandikumar, B. T. Goh, Y. S. Lim, W. J. Basirun, H. N. Lim and N. M. Huang, *R. Soc. Chem. Adv.*2015, **5** 14010-14019

[7] R. A. Patil, R. S. Devan, J. –H. Lin, Y. –R. Ma, P. S. Patil and Y. Liou, *Sol. Energ. Mat. Sol.* 2013, **112** 91-96.

[8] X. Wang, Y. Z. Li, S. Wang, Z. Zhang, L. Fei and Y. Qian, *Cryst. Growth Des.*2006, **6** 2163-2165.

[9] E. A. Gibson, M. Awais, D. Dini, D. P. Dowling, M. T. Pryce, J. G. Vos, G. Boschloo and A. Hagfeldt, *Phys. Chem. Chem. Phys.* 2013, **15** 2411-2420

[10] M. Tyagi , M. Tomar and V. Gupta, *Biosens. Bioelectron.* 2013, **41** 6.

[11] H. Wang, C. Du, P. C. Hammel and F. Yang, *Phys. Rev. Lett.* 2014, **113** 097202.

[12] H. Christian, De L. Grégoire, V. N. Vladimir, Ben Y. Jamal, K. Olivier and V. Michel, *Europhys. Lett.* 2014, **108** 57005.

[13] R.Vardimon, M. Klionsky and O. Tal, *Nano Lett.* 2015, **15** 3894-3898.

[14] Y. Jiang, D. Chen, J. Song, Z. Jiao, Q. Ma, H. Zhang, L. Cheng, B. Zhao and Y. Chu, *Electrochim. Acta* 2013,**91** 173-178.

[15] G. Zhou, D. –W. Wang, L. –C. Yin, N. Li, F. Li and H. –M. Cheng, *ACS Nano* 2012, **6** 3214-3223.

[16] X. Zhu, Q. Jiao, C. Zhang, X. Zuo, X. Xiao, Y. Liang and J. Nan , *Microchem. Acta* 2013, **180** 7.

[17] J. Saha and R. H. Victora, *Phys. Rev. B* 2007, **76** 100405.

[18] T. Maity, S. Goswami, D. Bhattacharya, G. C. Das and S. Roy, *J. Appl. Phys.* 2013, **113** 17D916.

[19] J. Van Lierop, K. W. Lin, J. Y. Guo, H. Ouyang and B. W. Southern, *Phys. Rev. B* 2007, **98** 237201.

[20] Chunting Liu, Ji Ma and Houyang Chen, *RSC Adv.* 2012, **2** 1009-1013.

[21] A. Hossein, S. Hadi, K. Parviz, P. Asok, A. Mehmet and Z. Khalil, *J. Phys. D: Appl. Phys.* 2010, **43** 245002.

[22] S. Chauhan, S. S. Kumar and R. Chandra, *Appl. Phys. Lett.* 2013, **103** 042416.

[23] A. C. Gandhi, J. Pant, S. D. Pandit, S. K. Dalimbkar, T. –S. Chan, C. –L. Cheng, Y. –R. Ma and S. Y. Wu, *J. Phys. Chem. C* 2013, *117* 18666-18674.

[24] E. Winkler, R. D. Zysler, M. V. Mansilla, D. Fiorani, D. Rinaldi, M. Vasilakaki and K. N. Trohidou, *Nanotechnology* 2008, **19** 185702.

[25] E. Winkler, R. D. Zysler, M. V. Mansilla and D. Fiorani, *Phys. Rev. B* 2005, **72** 132409.

[26] S.Thota and J. Kumar, *J. Phys. Chem. Solids* 2007, **68** 1951-1964.

[27] S. D. Tiwari, K. P. Rajeev, *Phys. Rev. B* 2005, **72** 104433.

[28] M. Ghosh, K. Biswas, A. Sundaresan, C. N. R. Rao, *J. Mat. Chem.* 2006, **16** 106-111.

[29] S. K. Sharma, J. M. Vargas, E. D. Biasi, F. Béron, M. Knobel, K. R. Pirota, C. T. Meneses, K. Shalendra, C. G. Lee, P. G. Pagliuso and R. Carlos, *Nanotechnology* 2010, **21** 035602.

[30] S. Haas, E. Dagotto, J. Riera, R. Merlin and F. Nori, *J. Appl. Phys.* 1994, **75** 6340-6342.

[31] Duan W. J. Duan, S. H. Lu, Z. L. Wuand Y. S. Wang, *J. Phys. Chem. C* 2012, **116** 26043-26051.

[32] N. Rinaldi-Montes, P. Gorria, D. Martinez-Blanco, A. B. Fuertes, Barquin L. Fernandez, Fernandez J. Rodriguez, I. de Pedro, M. L. Fdez-Gubieda, J. Alonso, L. Olivi, G. Aquilanti and J. A. Blanco, *Nanoscale* 2014, **6** 457-465.

[33] S. Mandal, K. S. R. Menon, S. K. Mahatha and S. Banerjee *Appl. Phys. Lett.* 2011, **99** 232507.

[34] J. T. Richardson, D. I. Yiagas, B. Turk, K. Forster and M. V.Twigg, *J. Appl. Phys.* 1991, **70** 6977-6982.

[35] M. P. Proenca, C. T. Sousa, A. M. Pereira, P. B. Tavares, J. Ventura, M. Vazquez and J. P. Araujo, *Phys. Chem. Chem. Phys.* 2011, **13** 9561-9567.

[36] M. Jagodič, Z. Jagličić, A. Jelen, Jin Bae Lee, Young-Min Kim, Hae Jin Kim and J. Dolinšek, *J. Phys. Condens. Matter* 2009, **21** 215302.

[37] S. Mandal, S. Banerjee and K. S. R. Menon, *Phys. Rev. B* 2009, **80** 214420.

[38] A. Gandhi, C. –Y. Huang, C. C. Yang, T. –S. Chan, C. –L. Cheng, Y. –R. Ma and S. Y. Wu, *Nanoscale Res. Lett.*2011, **6** 1-14.

[39] L. Néel , *Ann Geophys (C N R S)* 1949, **5** 37.

[40] W. Brown, *Phys. Rev.*1963, **130** 1677-1686.

[41] M. Ulrich, J. García-Otero, J. Rivas and A. Bunde, *Phys. Rev. B* 2003, **67** 024416.

[42] F. Rivadulla, M. A. López-Quintela and J. Rivas, *Phys. Rev. Lett.*2004, **93** 167206.

[43] K. De, S. Majumdar and S. Giri, *J. Phys. D: Appl. Phys.* 2007, **40** 5810.

[44] M. Thakur, M. P. Chowdhury, S. Majumdar and S. Giri, *Nanotechnology* 2008, **19** 045706.

[45] D. De, A. Karmakar, M. K. Bhunia, A. Bhaumik, S. Majumdar and S. Giri, *J. Appl. Phys.* 2012, **111** 033919.

[46] X. Chen, S. Sahoo, W. Kleemann, S. Cardoso and P. P. Freitas, *Phys. Rev. B* 2004, **70** 172411.

[47] Jhong-Yi Ji, Po-Hsun Shih, Ting-Shan Chan, Yuan-Ron Ma and Sheng Yun Wu, *Nanoscale Res. Lett.* 2015, **10** 243.

[48] T. Maity, S. Goswami, D. Bhattacharya and S. Roy, *Phys. Rev. Lett.* 2013, **110** 107201.

[49] J. Nogués, J. Sort, V. Langlais, V. Skumryev, S. Suriñach, J. S. Muñoz and M. D.Baró, *Phys. Rep.* 2005, **422** 65-117.

Figure Captions

Figures 1 (a)-(e) TEM images and (f)-(j) SAED patterns of the 16.6(7) to 54(6) nm NiO nanoparticles. The insets of Figure 1(a)-(e) show HRTEM images of the respective NiO nanoparticles.

Figures 2 (a) M(T) curves measured with the ZFC-FC protocol in an external magnetic field of 100 Oe for 16.6(7) nm NiO nanoparticles. (b) Blocking (T_B), irreversible (T_{irr}), and freezing (T_f) temperature as functions of nanoparticle size.

Figure 3 The T_B and K versus the volume of NiO nanoparticles. The black solid line indicates the fit to the experimental data obtained using the Néel-Brown models. The dashed exponential curve is a guide for the eye only.

Figure 4 Plot of ln(t) dependency of lnW(t) measured from all the NiO samples. The straight line shows the a model fit (see the text) to the experimental data after the lapse of a crossover time t_o

Figures 5 (a)-(e) A portion of the $M(H_a)$ loop near the origin of the hysteresis loop measured at 25 K with *p*-and *n*-type protocols after zero-field cooling for 16.6(7) to 54(6) nm NiO nanoparticles, respectively. The dashed red colored line represents the virgin magnetization curve. (f) Measured H_{SEB} field 25 K as a function of the crystalline size of the nanoparticles.

Figures 6 (a)-(d) shows the variation in H_{SEB}, H_C, M_{VS}, and M_r for different size nanoparticles as a functions of temperature.

Table 1 Summary of the freezing temperature (T_f), anisotropic temperature (T_l), blocking temperature (T_B), irreversible temperature (T_{irr}) and the anisotropy energy density (K) of various sized NiO nanoparticles.

T_A (°C)	Size (nm)	T_f (K)	T_B (K)	T_{irr} (K)	K (erg/cm^3)
400	16.6(7)	6	178	262	225852
500	19.5(6)	6	198	325	154985
600	29(4)	6	306	384	72821
700	31(1)	6	374	398	72864
800	54(6)	…..	…..	….	……

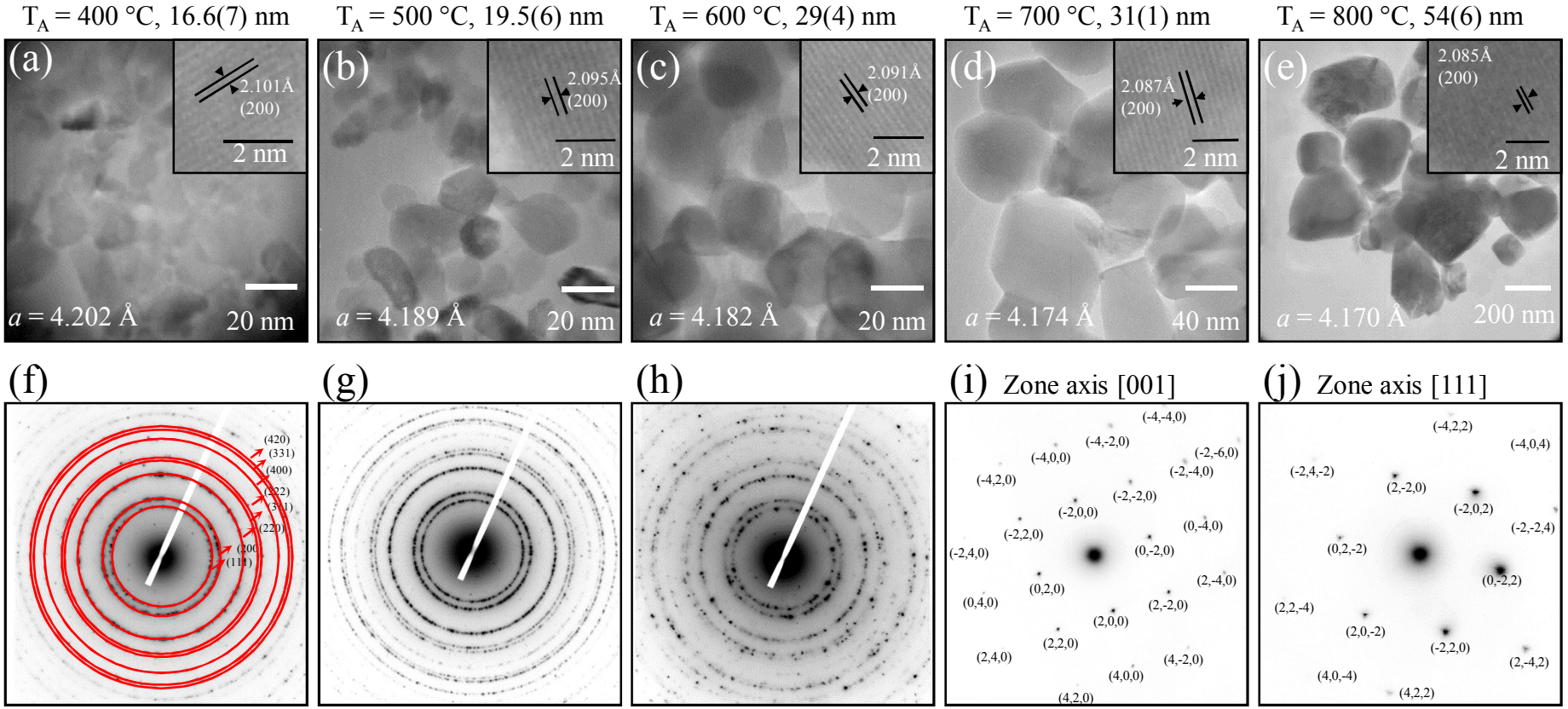

Figure 1 A. C. Gandhi *et al.*

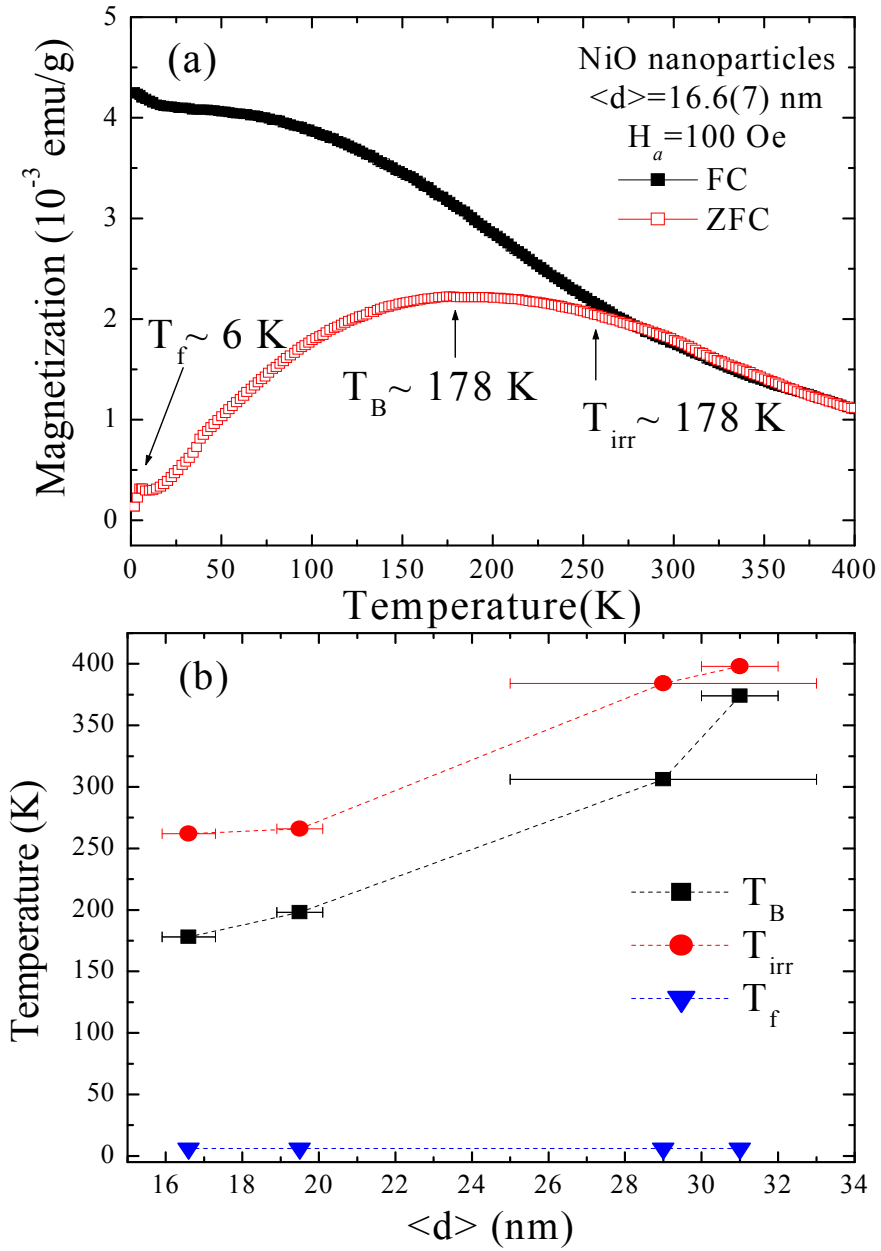

Figure 2 A. C. Gandhi *et al.*

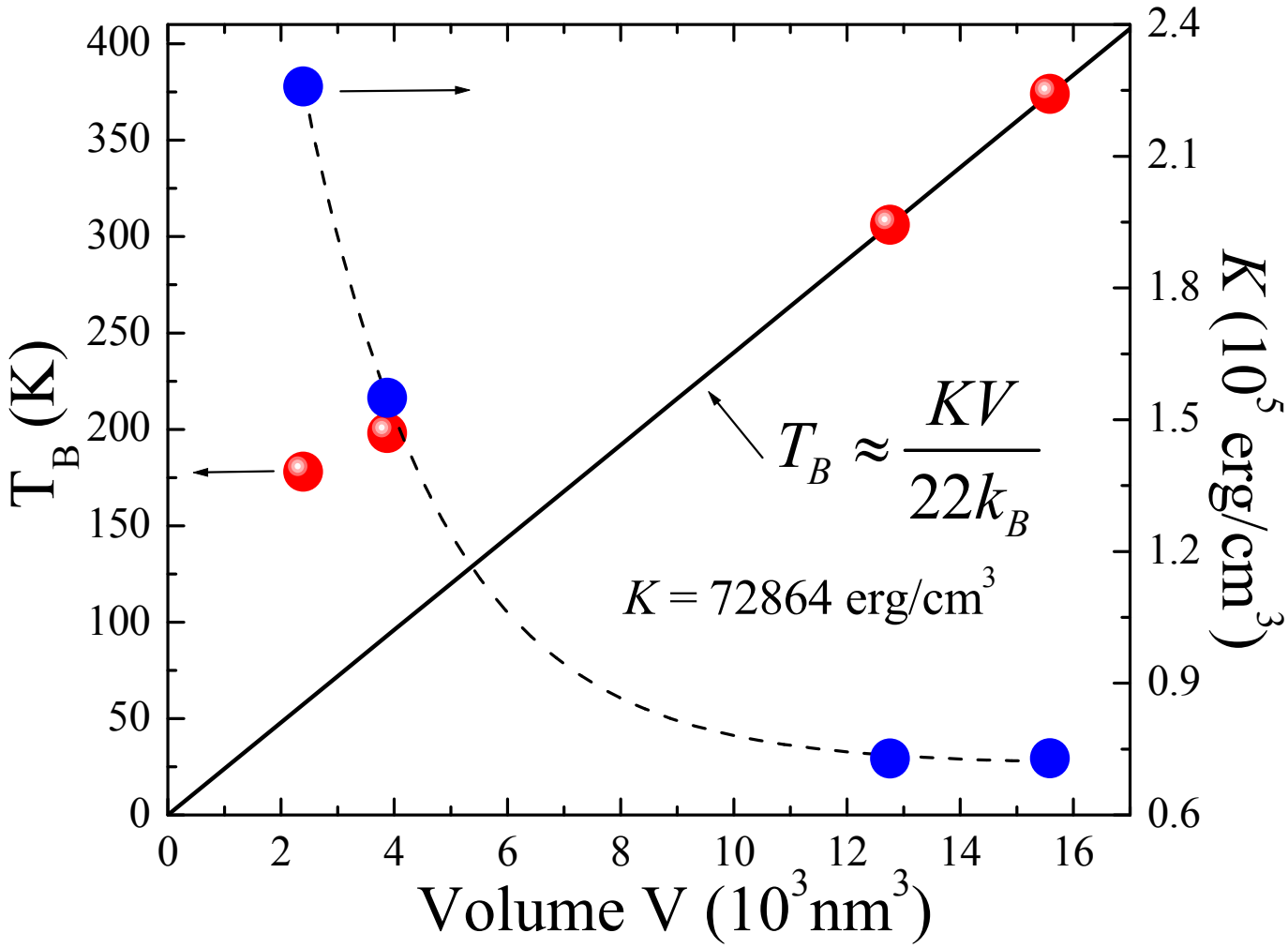

Figure 3 A. C. Gandhi *et al.*

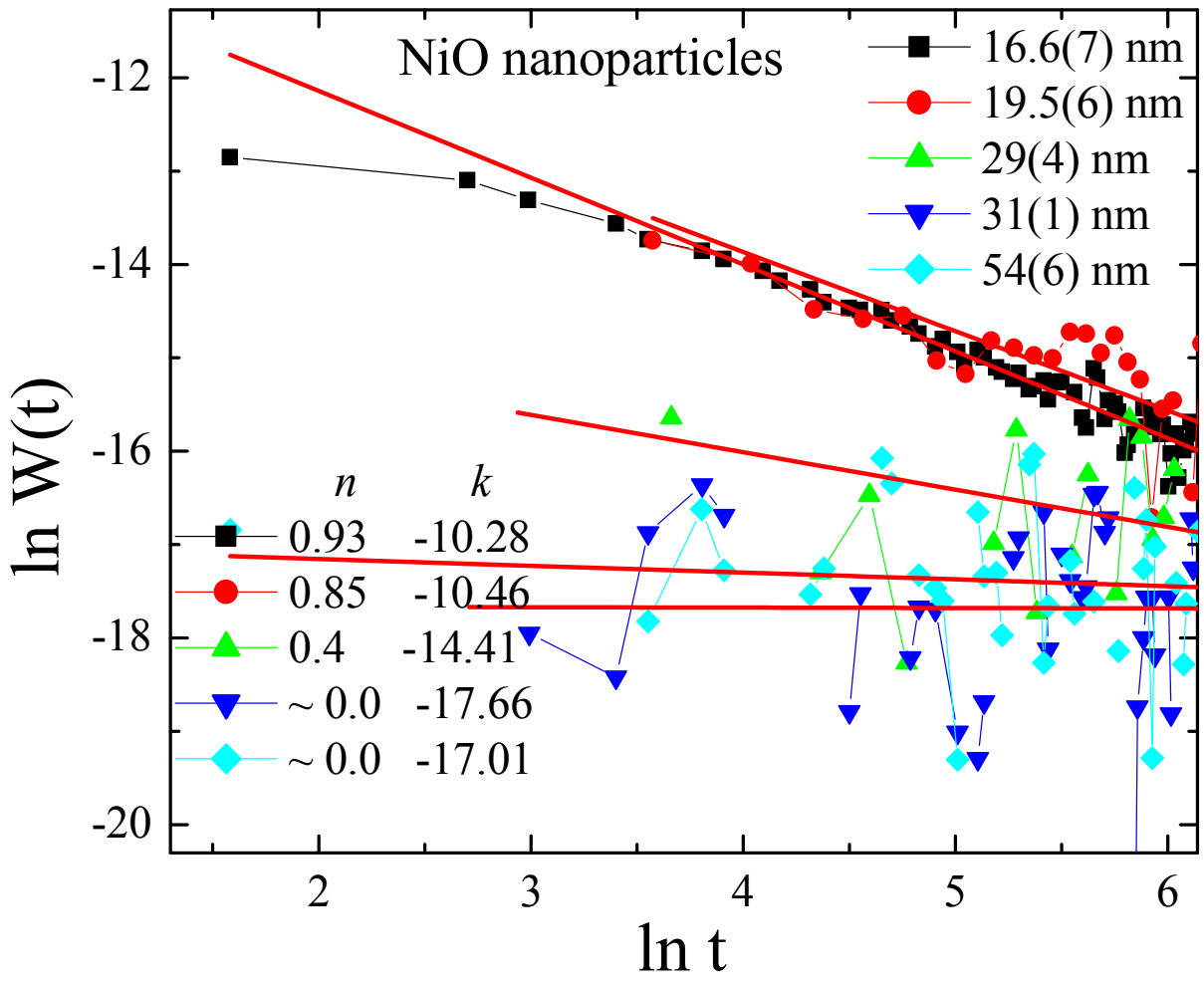

Figure 4 A. C. Gandhi *et al.*

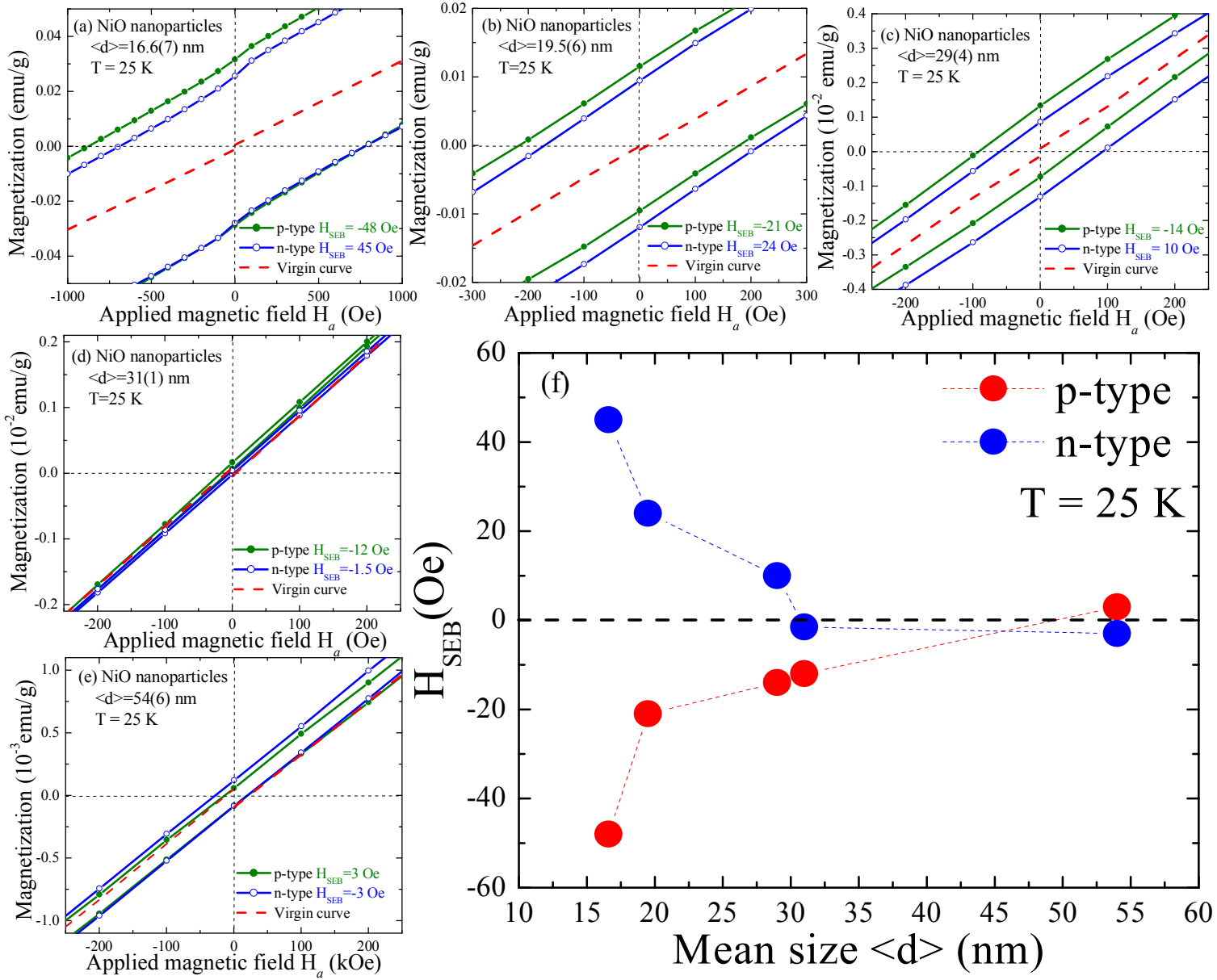

Figure 5 A. C. Gandhi *et al.*

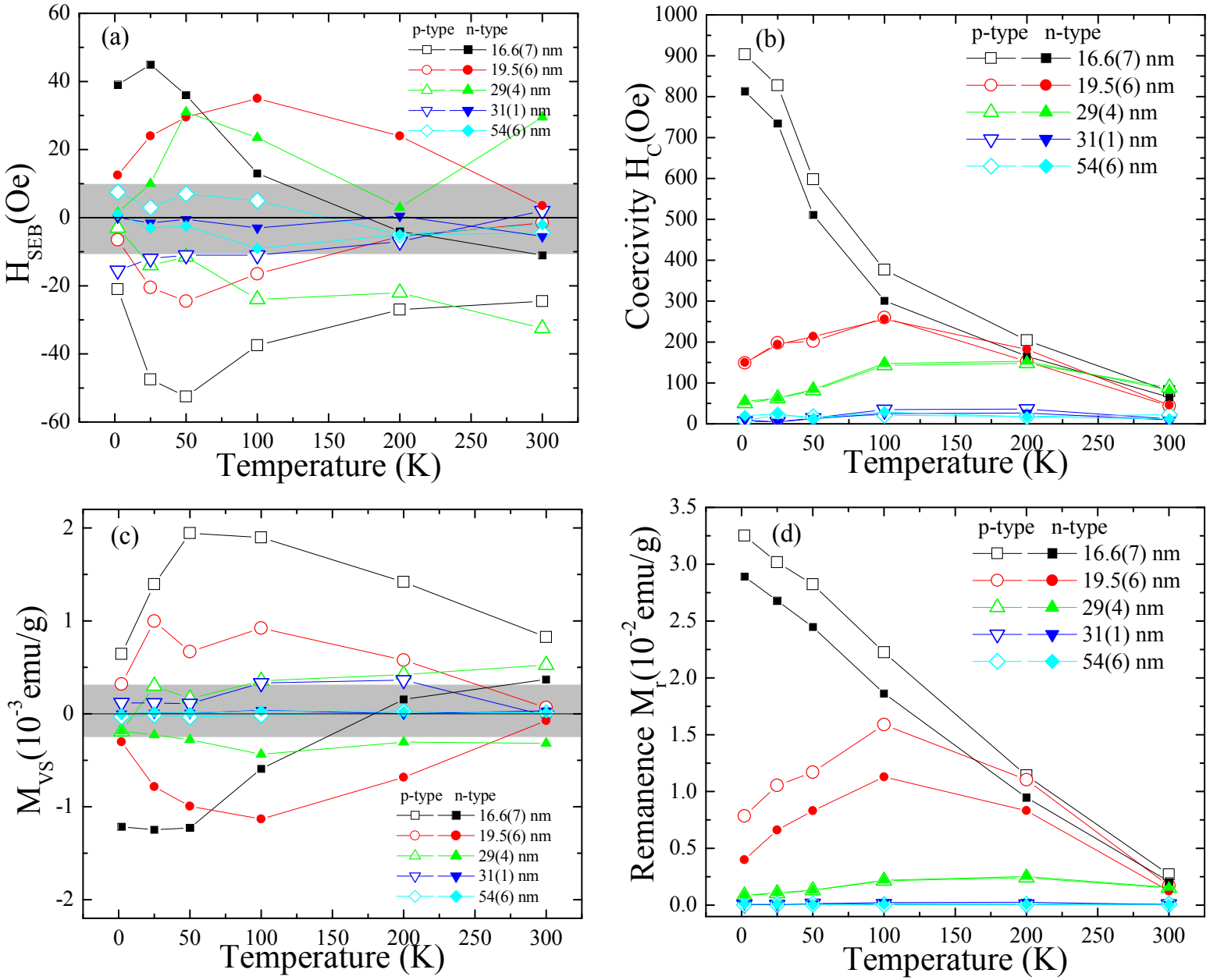

Figure 6 A. C. Gandhi *et al.*

Table of content

Dense Inter-particle Interaction Mediated Spontaneous Exchange Bias in NiO Nanoparticles

Ashish Chhaganal Gandhi, Jayashree Pant, and Sheng Yun Wu

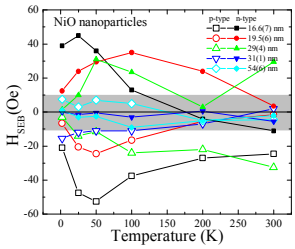

The observed spontaneous exchange bias in NiO nanoparticles is induced by the dense inter-particle interactions.